

DESIGN OF MEDICAL RADIOMETER FRONT-END FOR IMPROVED PERFORMANCE

Ø. Klemetsen, Y. Birkelund, and S. K. Jacobsen

Department of Physics and Technology
University of Tromsø, NO-9037 Tromsø, Norway

P. F. Maccarini and P. R. Stauffer

Duke University Medical Center
2301 Erwin Road, Durham, NC 27710, USA

Abstract—We have investigated the possibility of building a singleband Dicke radiometer that is inexpensive, small-sized, stable, highly sensitive, and which consists of readily available microwave components. The selected frequency band is at 3.25–3.75 GHz which provides a reasonable compromise between spatial resolution (antenna size) and sensing depth for radiometry applications in lossy tissue. Foreseen applications of the instrument are non-invasive temperature monitoring for breast cancer detection and temperature monitoring during heating. We have found off-the-shelf microwave components that are sufficiently small ($< 5 \text{ mm} \times 5 \text{ mm}$) and which offer satisfactory overall sensitivity. Two different Dicke radiometers have been realized: one is a conventional design with the Dicke switch at the front-end to select either the antenna or noise reference channels for amplification. The second design places a matched pair of low noise amplifiers *in front* of the Dicke switch to reduce system noise figure.

Numerical simulations were performed to test the design concepts before building prototype PCB front-end layouts of the radiometer. Both designs provide an overall power gain of approximately 50 dB over a 500 MHz bandwidth centered at 3.5 GHz. No stability problems were observed despite using triple-cascaded amplifier configurations to boost the thermal signals. The prototypes were tested for sensitivity after calibration in two different water baths. Experiments showed superior sensitivity (36% higher) when implementing the low noise amplifier *before* the Dicke switch (close to the antenna) compared to the

other design with the Dicke switch in front. Radiometer performance was also tested in a multilayered phantom during alternating heating and radiometric reading. Empirical tests showed that for the configuration with Dicke switch first, the switch had to be locked in the reference position during application of microwave heating to avoid damage to the active components (amplifiers and power meter). For the configuration with a low noise amplifier up front, damage would occur to the active components of the radiometer if used in presence of the microwave heating antenna. Nevertheless, this design showed significantly improved sensitivity of measured temperatures and merits further investigation to determine methods of protecting the radiometer for amplifier first front ends.

1. INTRODUCTION

It is well known that microwave radiometry can be used for noninvasive temperature measurements of superficial tissue in the human body. As opposed to other active methods that stimulate the body with some kind of excitation signal, radiometry is passive and thus completely harmless. Over the past four decades, research within the field of microwave radiometry has been conducted for use in medical applications [1]. Modalities under investigation include detection of breast cancer [2], thermal monitoring of hyperthermia, and detection of inflammation [3]. In medical treatment involving microwave heating of the body, there is a need for temperature observation of the heated tissue. While conventional microwave-immune probes (e.g., fiberoptics) may be placed on the skin surface and/or implanted into tissue through catheters to monitor temperature, an accurate and convenient method for non-invasive temperature monitoring is preferred.

Russian scientists have developed a radiometer for the detection of breast cancer which is manufactured under the name of RTM-01[†]. The technical details of this radiometer are not known, and are therefore difficult to evaluate. However, the detection procedure is to make corresponding point measurements of both breasts and assess asymmetries in measured brightness temperatures.

Vesicoureteral reflux (VUR) is an abnormal movement of urine from the bladder into the ureters and kidneys, and is a significant health problem. Younger children are more prone to VUR because of the relative shortness of the submucosal ureters. This susceptibility decreases with age as the length of the ureters increases. In children under the age of 1 year with a urinary tract infection, more than

[†] <http://www.resltd.ru/eng/rtm/>.

the half will suffer from VUR[‡]. Current methods of imaging reflux rely on X-ray fluoroscopy of the kidneys after injection of radioactive contrast agent into the bladder via Foley catheter. X-ray exposure and use of invasive catheters are preferably avoided in children. An alternative procedure has been proposed in which the reflux of urine can be detected by warming the bladder with microwave radiation to a fever temperature and measuring kidney temperatures with a microwave radiometer to detect temperature rise in the kidney after reflux [4]. In addition to monitoring the kidneys for reflux, a microwave radiometer could also be used to passively monitor bladder temperature during microwave heating. This study investigates the construction of a miniature radiometer to read volume-averaged temperature of superficial tissue.

Microwave radiometers can be assembled in different ways. The two most common variants are total power radiometer and Dicke radiometer [5]. A total power radiometer consists of a medium gain low noise amplifier (LNA), followed by a booster amplifier and a power meter or a square law detector as well as an integrator. This radiometer is very sensitive to amplifier drift. A Dicke radiometer uses a switch in front of the LNA to select between the sensing antenna and a known noise reference, as shown in Fig. 1. When switching faster than the gain variations, these unwanted drift effects are mostly canceled out [6].

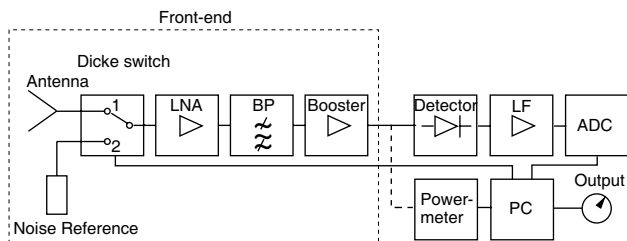


Figure 1. Block diagram of Dicke radiometer.

The goal of the present design is to determine whether it is possible to create an inexpensive and small sized front stage of a radiometer using available commercial surface mount device (SMD) components while meeting the design requirements of useful medical radiometry. Pertinent design requirements are stability against oscillations and adequate sensitivity for radiometric detection of $3 - 5^{\circ}\text{C}$ temperature rise at a depth of at least 30 mm in tissue. It has previously been shown that active antennas with LNA before the Dicke switch improve the overall thermal sensitivity of the radiometer [7]. Presently, we

[‡] <http://kidney.niddk.nih.gov/statistics/uda/>.

investigate a generalization of this concept by implementing LNAs before the Dicke switch for both the antenna input and the reference signal. In this way we get a more balanced Dicke radiometer with further improvement in accuracy of observed brightness temperature.

2. THEORETICAL BACKGROUND

A microwave radiometer is an instrument that can measure temperatures inside the human body. The measuring principle is to quantify the thermally emitted power over a given frequency band. Blackbody spectral radiance at temperature T is for all frequencies given by Planck's radiation law. Planck's law can be approximated by Rayleigh-Jean's law in the microwave band, and from which the noise power P over a frequency band Δf can be written [6]:

$$P = kT\Delta f, \quad (1)$$

where k is Boltzmann's constant.

Relating this principle to practical multi-stage radiometric systems, the theoretical noise temperature T_e of a cascaded system is given by:

$$T_e = T_{e1} + \frac{T_{e2}}{G_1} + \frac{T_{e3}}{G_1 G_2} + \dots + \frac{T_{eN}}{G_1 G_2 \dots G_{N-1}} \quad (2)$$

where $T_{e,i}$, G_i are the noise temperature and gain of the individual stages, respectively. From Eq. (2) the noise performance of the first stage is critical. This inherent property is often utilized in measurement systems through implementation of low-noise preamplifiers close to the sensor element. The theoretical sensitivity of an ideal total-power radiometer with no gain fluctuations is [6]:

$$\Delta T = \frac{T_a + T_e}{\sqrt{\Delta f \tau}}, \quad (3)$$

where ΔT is the minimum detectable change in the radiometric antenna temperature T_a and τ is the integration time in the low pass filter (integrator). For a Dicke radiometer (Fig. 1), the theoretical sensitivity is given by:

$$\Delta T_{\min} = \frac{2(T_a + T_e)}{\sqrt{\Delta f \tau}}. \quad (4)$$

Since the integration time τ has to be divided between the reference and the antenna, the Dicke radiometer provides a degradation of ΔT (factor 2) compared to the total power radiometer.

A conventional digital Dicke radiometer front-end consists of an antenna, a noise reference, a Dicke switch, a low noise amplifier, a

bandpass filter (BP), and a booster amplifier. Other parts are a square law detector, a low frequency (LF) amplifier, an analog to digital converter (ADC) and a controller PC. Alternatively, a power meter can be connected to the front-end. With the Dicke switch attached permanently to the antenna, the radiometer can be reconfigured to a total power radiometer.

A stable amplifier cascade configuration is important in order to avoid internal oscillations that might interfere with the extremely low radiated power received by the antenna. The stability of a system can be evaluated using the Edward-Sinsky stability factor defined as [8]:

$$\mu = \frac{1 - |S_{11}|^2}{|S_{22} - S_{11}^* \cdot \Delta| + |S_{12} \cdot S_{21}|} > 1 \quad (5)$$

where S_{ij} and Δ are elements and the determinant of the system parameter matrix \mathbf{S} , respectively. The system is unconditionally stable if $\mu > 1$.

While the commonly used standard deviation provides a measure of overall signal variations, it does not distinguish random noise from other typical signal drift types. On the other hand, the Allan deviation method has potential to differentiate between white noise, flicker noise (1/f-noise), random-walk drift as well as systematic long term signal drift [9]. Land et al. [10] used the Allan deviation to analyze the signal behavior of two different types of microwave radiometers.

The Allan deviation seeks to quantify temporal measurement variations within a time series and is defined as [11]:

$$\sigma_T(\tau) = \sqrt{\frac{\langle (\bar{T}_{k+1} - \bar{T}_k)^2 \rangle}{2}} \quad (6)$$

where $\bar{T}_k = (1/\tau) \int_{t_k}^{t_k+\tau} T(t) dt$ and $t_{k+1} = t_k + \tau$ for $k = 0, 1, \dots, \tau$.

Different spectral noise components appear with separate spectral density power laws in a log-log plot of the Allan deviation versus the sampling period τ . Hence, different types of noise can be distinguished by the slope of the plot in various time regions. For microwave radiometry, pertinent types of signal variations are [10]: i) Gaussian noise (slope of -0.5), ii) Flicker (1/f-) noise (slope of 0), iii) Random-walk noise (slope of 0.5), and iv) long term steady drift (slope of 1).

3. RADIOMETER DESIGN

Equation (1) shows that the noise power P depends primarily on the temperature T and bandwidth Δf . For human body temperatures, and for a practical bandwidth of say 500 MHz, the noise power over

that bandwidth is very low (-86.7 dBm). To detect this low power, it is crucial to have a sensitive instrument like a radiometer. From previous work [7], we have found that the frequency band around 3.5 GHz is a quiet band less disturbed by EMI compared to other low-GHz frequency communication bands. This frequency range provides smaller penetration depth in the human body compared to lower frequencies. However, the band has been shown as an adequate choice for detecting superficial breast cancer [12].

One challenge in the design phase is to find an LNA balancing the trade offs between lowest possible noise, highest possible gain, low power consumption and low cost. Several LNAs were considered with the best option from Hittite Microwave Corporation[§]. In order to isolate the front-end from other competing signal sources, we used a bandpass filter which is a combination of low pass (LP) and high pass (HP) filters from Mini-Circuits^{||}. The configuration gave an appropriate 500 MHz bandwidth. The steep slopes of the frequency cutoff at the edges of the pass band filter were enhanced by the use of two pairs of consecutive filters of the same type. Another design challenge was to identify a Dicke switch with lowest possible insertion loss, high isolation, 3.25–3.75 GHz bandwidth, small sized, and with single supply voltage. Our choice was a switch from Mini-Circuits[¶]. The switch requires a DC block capacitor of 47 pF before and after. Presently a capacitor from Murata Manufacturing Co., Ltd⁺ was used.

Table 1. Specifications of SMD components.

Device	Name	G [dB]	NF [dB]	T_e [K]	f [GHz]
LNA	HMC593LP3E	19	1.2	92.3	3.3–3.8
BP (LP part)	LFCN-3400+	-1.03	1.03	77.6	0–3.4
BP (HP-part)	HFCN-3100+	-1.01	1.01	75.9	3.4–9.9
Dicke switch	CSWA2-63DR+	-1.2	1.2	92.3	0.5–6
Capacitor	GQM1885C1H470JB01	-0.014	0.014	0.94	3.5

A single LNA does not provide enough gain to get the power into the required range for any power detector. Based on the component specifications listed in Table 1 for the LNA, filters and switch, we found that a configuration of three cascaded LNAs (3×19 dB) and four filters (4×-1 dB insertion loss) should give a suitable amplification in the selected frequency range. The bandpass filters give a theoretical bandwidth of $\Delta f = 500$ MHz.

[§] <http://www.hittite.com/>.

^{||} <http://www.minicircuits.com/>.

[¶] <http://www.minicircuits.com/>.

⁺ <http://www.murata.com/>.

3.1. Design Options

Many factors may degrade the RF stage in radiometers. This includes oscillations in amplifiers (stability), system noise, temperature- and gain drift as well as electromagnetic interference (EMI). An optimum radiometer front-end provides high sensitivity, low noise temperature, is unconditionally stable, has low gain drift, and yields marginal self-heating of surface mounted components. In a testing phase, a Dicke front-end radiometer should also be possible to run as a total power radiometer for comparison with other solutions. A complete radiometer can be designed in several ways. We want to realize the Dicke concept using a powermeter and a PC with LabView as a post-detector driver of the Dicke switch. This basic design was initially simulated with two options. Design #1: Conventional Dicke radiometer with a DC block capacitor and a Dicke switch in front, one LNA, a bandpass filter and two LNAs in cascade as booster amplifiers (see Fig. 2). Design #2: A modified Dicke radiometer with an LNA in front, a switch, two cascaded LNAs and a bandpass filter (see Fig. 3). The last design does not require DC block capacitors because of an internal DC block in the LNA. Both radiometers have been characterized using the following performance indices: *S*-parameters, system noise figures [Eq. (2)], sensitivity [Eq. (3)], stability factors [Eq. (5)], together with the average and standard deviation of a known temperature source.

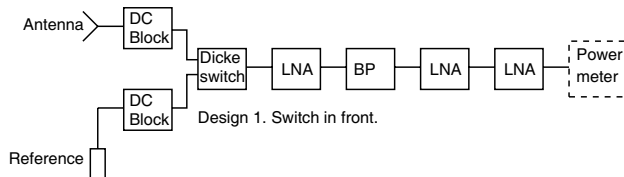


Figure 2. Block diagram of design #1.

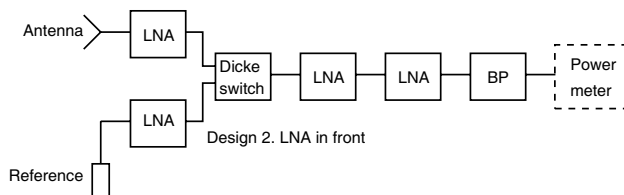


Figure 3. Block diagram of design #2.

Table 2. Performance indices of radiometric designs. Integration time: $\tau = 2.0$ s for theoretical sensitivity. $\tau = 2.77$ s for measured sensitivity.

	Parameter	design #1	design #2
Theoretical system noise temperature	T_e	217.2 K	95.1 K
Simulated noise power from S -parameters	P_s	-34.25 dBm	-34.01 dBm
From measured S -parameters	P_{sm}	-35.26 dBm	-33.40 dBm
Measured noise power	P_m	-33.50 dBm	-32.80 dBm
Theoretical sensitivity, total power radiometer	ΔT	0.016 K	0.012 K
Theoretical sensitivity, Dicke radiometer	ΔT_{\min}	0.032 K	0.024 K
Measured sensitivity, total power radiometer	ΔT	0.064 K	0.046 K
Measured sensitivity, Dicke radiometer	ΔT	0.098 K	0.062 K

4. RESULTS

4.1. Simulations

In the simulations based on CST Design Studio*, S -parameters were given by touchstone files from the component manufacturer's web sites. Numerical simulations were performed by importing individual touchstone files for every single block in the design, and generating the overall S -parameters of the circuit in the frequency range from 1 to 6 GHz. T_e for each design was derived from the theoretical noise temperature of a cascaded system given by Eq. (2) combined with parameters in Table 1. The expected output power from the system when using an antenna temperature $T_a = 290$ K was determined by integrating over frequencies in the simulated system $|S_{21}|^2$ and multiplying by $k(T_a + T_e)$, given by Eq. (1). The simulated power in dBW is thus: $P_s = 10 \log[\sum |S_{21}|^2 k(T_a + T_e)]$. The theoretical noise temperatures using Eq. (2), expected output power, and sensitivity using Eqs. (3) and (4) are listed in Table 2.

* <http://www.cst.com>.

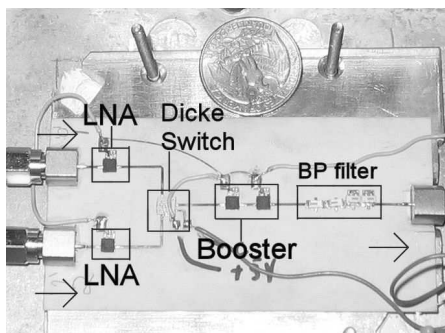


Figure 4. Picture of PCB design with LNA in front.

4.2. Prototype Testing

The prototype design was realized with a printed circuit board (PCB) RO4350B, (Rogers Corp., USA)[#] of 0.254 mm thickness and a copper layer of 35 microns (see Fig. 4) for the design with the LNA in front. The system was tested by an Agilent E5071C network analyzer and an Agilent E4419B power meter containing an E4412A sensor. The Dicke switch is controlled by a USB-3114 device from Measurement Computing, USA^{††}. The measurements were undertaken with the front-end blocks as shown in Fig. 1 and shown in detail in Figs. 2 and 3. Experimental values were generated for touchstone files from the network analyzer and thereafter the stability factor μ and the expected output power P_{sm} were calculated.

Time-series measurements were conducted with a $50\ \Omega$ load as a thermal source of temperature $T_a = 290\ \text{K}$. The system performance was monitored over time by logging power P_m together with other system parameters. The results are listed in Table 2. The simulated and measured forward transmission S_{21} and stability factor μ are depicted in Fig. 5 for the two designs. The input reflection coefficient S_{11} and output reflection coefficient S_{22} are shown in Fig. 6.

Sensitivity of the radiometer design was found by calibrating the radiometers with two different and known temperatures, T_h , T_c , in a water bath. The calibration parameter $s = \frac{P_h - P_c}{T_h - T_c}$ is the slope of the output power P_h and P_c as a function of temperatures T_h and T_c . The sensitivity could then be determined from $\Delta T = \frac{\sigma_{P_o}}{s}$. σ_{P_o} is the measured standard deviation to the measured output power P_o . Numerical values are given in Table 2. The Dicke concept was also

[#] <http://www.rogerscorp.com/>.

^{††} <http://www.mccdaq.com>.

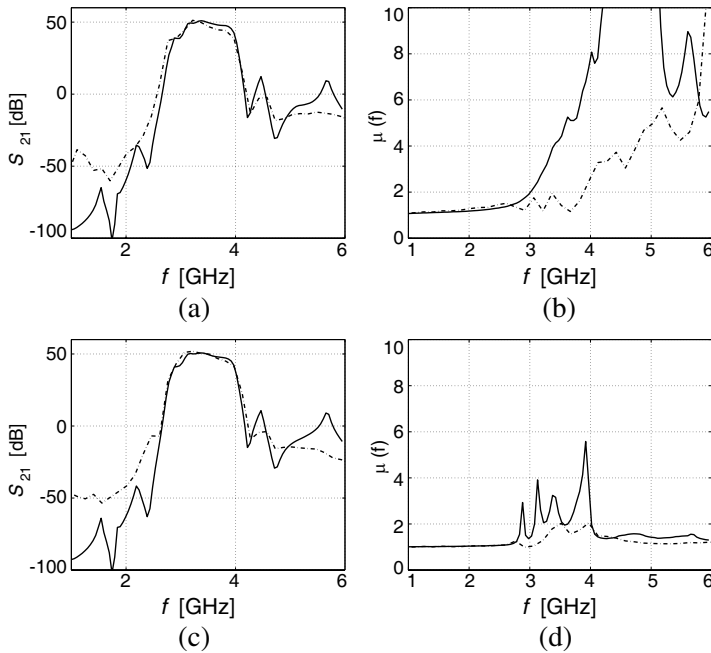


Figure 5. S_{21} and μ for design #1, (upper panels) and design #2 (lower panels). Solid line: Simulated values. Dotted line: Measured values. (a) Design #1, S_{21} . (b) Design #1, μ . (c) Design #2, S_{21} . (d) Design #2, μ .

tested for gain variations caused by temperature changes of the chassis using a Peltier element for heating and by changing the supply voltage (see Fig. 7).

Finally, the noise statistics were analyzed for the radiometer using the Allan deviation defined in Eq. (6). Fig. 8 depicts a typical time series of more than two hours of radiometric data. From visual inspection we observe in Fig. 8(a) a slow decrease of average power value over time. The corresponding Allan deviation estimate is shown in Fig. 8(b) and further discussed in the next section.

4.3. Experimental Testing of Radiometer Performance

The radiometers were further tested with a fully automated system for interspersed heating and radiometric reading on a layered solid phantom (see Fig. 9). The stacked phantom consisted of a 5 mm fat layer on top, a 28 mm muscle phantom in the middle and a

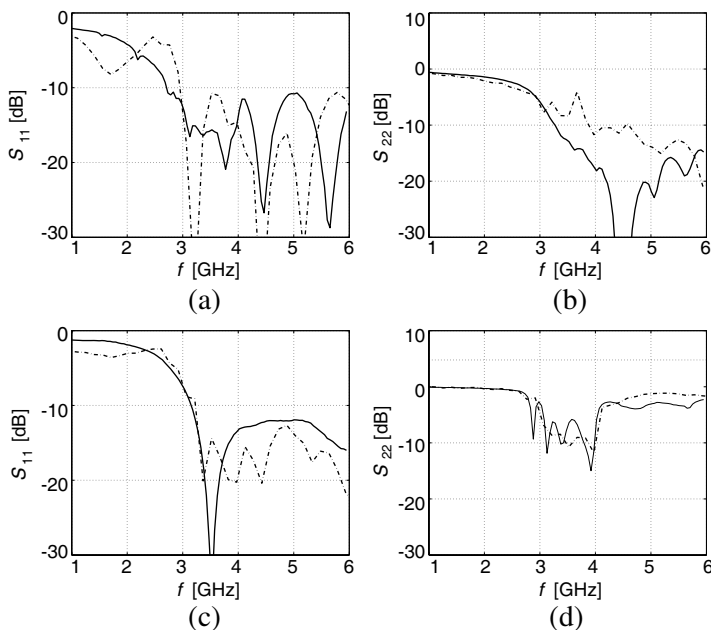


Figure 6. S_{11} and S_{22} . Solid line: Simulated values. Dotted line: Measured values. (a) Design #1, S_{11} . (b) Design #1, S_{22} . (c) Design #2, S_{11} . (d) Design #2, S_{22} .

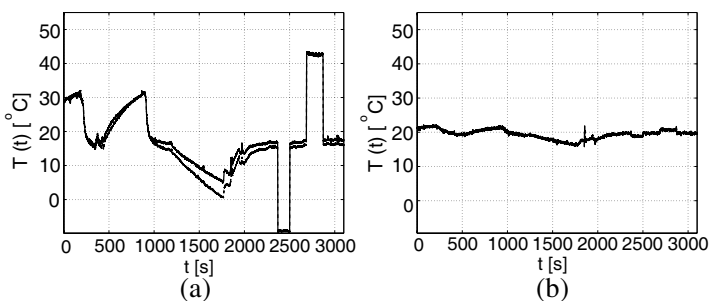


Figure 7. Stability analysis of Dicke concept for design #2 with an integration time $\tau = 3.1$ s. (a) The first part between 0 to 2300 s is the chassis temperature change with a Peltier element of the radiometer. The last part between 2300 to 3100 s is a power supply change of $\pm 2\%$. (b) The calibrated Dicke difference output.

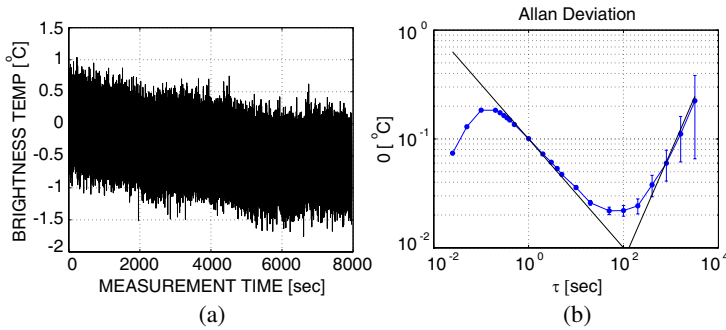


Figure 8. Signal noise and drift variations analyzed by the Allan deviation. Slopes of solid lines in b) are -0.5 and 1.0 . (a) Low drift radiometric data. 454 Hz sampling rate and post-processing integration time of 0.1 secs. (b) Allan deviation vs integration time.

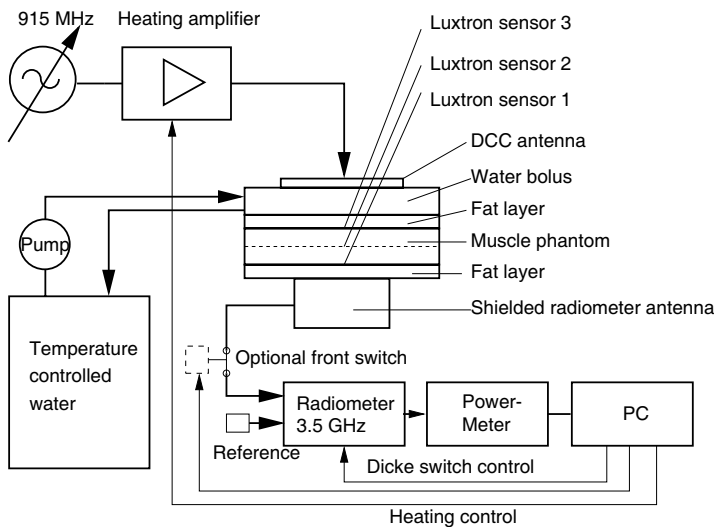


Figure 9. Experimental microwave heat and radiometric reading.

5 mm fatlayer at the bottom. Heating was done with a single Dual Concentric Conductor (DCC) antenna [13, 14] at 915 MHz through a bolus of circulating water. The input power to the top antenna was approximately 20 W at 915 MHz. Radiometric readings (see Fig. 10) with design #1 were obtained on the bottom surface with a shielded [4] elliptical antenna [15]. The temperature within the muscle phantom was also monitored with Luxtron (LumaSense Technologies) fiberoptic

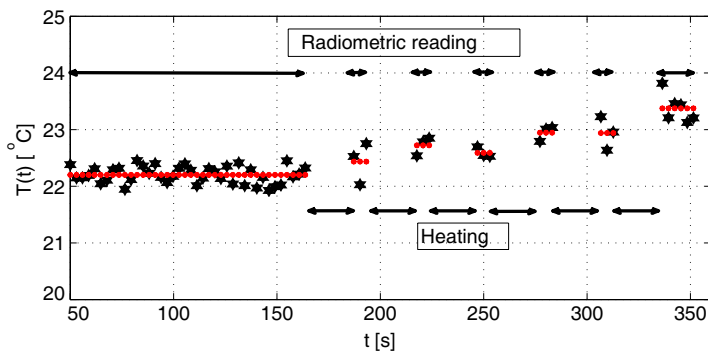


Figure 10. Radiometric reading with design #1 during protocol with interspersed 20 s heating with 915 MHz DCC antenna at 20 W and 10 s reading with power off. Integration time $\tau = 3$ s. Standard deviation, $\sigma = 0.15^\circ\text{C}$ before heating. Red dots are the mean value of the radiometric reading.

probes. The heating protocol was heating for 20 s with 20 W and reading for 10 s with heating turned off. After six heating cycles, the spatial temperature distribution inside the phantom was generated with an infrared camera (see Fig. 12).

5. DISCUSSION

Two distinct designs of a small sized ($45 \times 90 \text{ mm}^2$) frontend radiometer are demonstrated. The proposed designs gave the expected gain over the selected frequency band (3.25–3.75 GHz). Both designs were stable as the stability factor $\mu > 1$ for all frequencies for both simulated and measured data. The input reflection coefficient S_{11} is in the expected range (Fig. 6). The output reflection coefficient S_{22} for design #1 has a peak at the center frequency 3.5 GHz, and care must be taken in the following stage, usually a square law detector, in order to avoid signal instabilities. The noise temperature T_e was better for design #2 compared to design #1. This was anticipated as a consequence of lower overall noise figure, since the first LNA in design #2 has a gain of 19 dB and a noise factor of only 1.2 dB.

The selected thickness of the PCB is a challenge, because soldered connectors are easily broken apart from the PCB. Future designs require a multi-layer PCB for better mechanical stability. Although the design is chosen for minimum power consumption, it requires a heat sink to minimize influence from ambient temperature changes that may induce temperature variations on the PCB and thus gain

drift. In the design where LNAs precede the reference and antenna input, it is important that these components are well matched and drift synchronously, as the Dicke concept is not valid for this dual amplifier design.

Sensitivity of the prototype was worse than expected and is probably due to manual soldering of SMD components with more solder flux than in a professional soldering process. However, the design with the low noise amplifier before the Dicke switch for both antenna and reference input, produced 36% better sensitivity than the design where the Dicke switch is in front. From Fig. 7, we conclude that the Dicke concept is working as expected but care must be taken to maintain constant power supply values and chassis temperature. The output from the Dicke radiometer remains more stable when either changing the temperature of the radiometer or the supply voltage than the totalpower radiometer output. The correlation coefficient between the two totalpower radiometer output channels was measured to 0.9904. The radiometer was calibrated at a stable operating voltage of 5 V. By changing the operating voltage, calibration will not be valid since there operation conditions have been altered for the system. Nevertheless, this gives an indication of how sensitive the radiometer is for changes in operating voltage.

Allan deviation can provide differentiation between various types of noise-like and coherent signals embedded in the radiometric response. From the log-log plot in Fig. 8(b), the following interpretation can be made in three time regions: (i) Between 0.25 to 10 s the white noise (uniform spectral density) is dominant following the predicted -0.5 slope, (ii) the roll-off below 0.1 s is the convolution of the post-detector integration filter (cut-off frequency of 10 Hz) with the raw radiometric data sampled at 454 Hz, (iii) above 200 s the Allan deviation follows a slope of 1.0 indicating a systematic drift during the measurement time. This is confirmed through a linear fit in Fig. 8(a) which gives mean drift rate over the acquisition time of $87 \mu\text{Ks}^{-1}$. Flicker noise is a type of electronic noise with a $1/f$ (pink spectrum) spectral response that is present in almost all electronic devices. Presently, these devices include amplifying and detecting components. If significant, this form of noise contribution should show up as a constant plateau (slope of 0) in a given time region. Based on Fig. 8(b), we conclude that this type of noise is negligible (not detectable) compared to the other two types discussed above. Finally, random-walk noise originating from short-term temperature changes inducing variable losses and amplifier gains was neither identified (slope of 0.5) in the Allan deviation plot.

During the heating sequence (Fig. 9), the Dicke switch has to be

locked in the reference position to avoid damage of radiometer and power meter. Dicke design #1 can thus be used during heating since the switch provides isolation of the front end. Furthermore, Dicke design #2 shows better sensitivity, but goes into saturation during heating. To avoid saturation of the first LNA, one can try to operate it in bypass mode during heating in future designs.

The possibility to read temperatures non-invasively inside an object during heating was also demonstrated. Results in Fig. 10 of radiometer design #1 show that the sensitivity in the experimental verification is worse than observed in the prototype testing (Table 2). The difference is likely due to the fact that the experimental test was done with a real sensor, an antenna, and not an ideal $50\ \Omega$ load. With an antenna as a load, EMI can be significant as no shielding room was used during the experiment. Another plausible explanation is noise produced in the cable between antenna and radiometer. Fig. 11 shows the true temperature at depth with the radiometric reading for comparison, and this is verified by the infrared images in Fig. 12. The temperature change during heating is not given by the same amount in the radiometer temperature reading (Fig. 10). This is because of phantom attenuation and the limited penetration ability for the higher frequencies at 3.5 GHz. Hence the microwave radiometer measures a single brightness temperature that is proportionate to the volumetric temperature distribution. To find the temperature at depth, the inverse problem has to be solved [16].

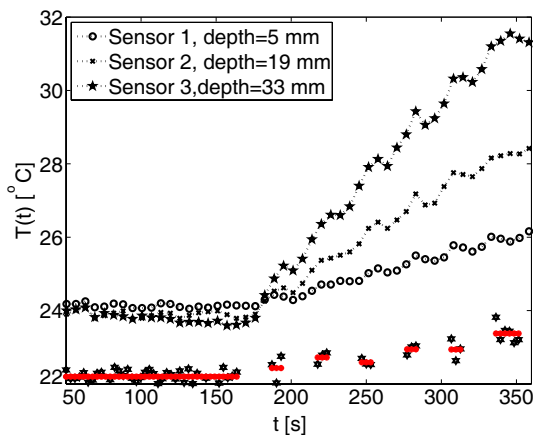


Figure 11. Temperature reading with Luxtron probes 1, 2 and 3 during heating. Depth is from the radiometric antenna. The radiometric reading is also plotted for comparison with the Luxtron temperature reading.

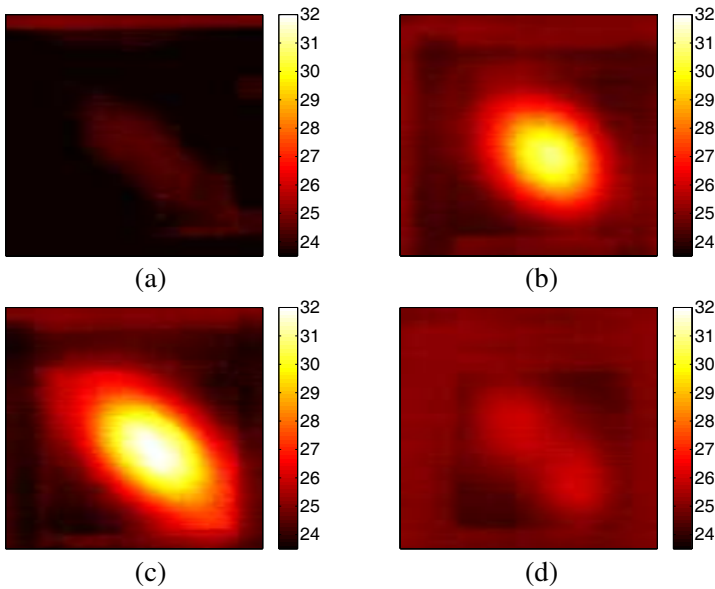


Figure 12. Infrared images after heating. Depth is from the radiometric antenna. (a) Depth 5 mm. $T_{\max} = 24.7^{\circ}\text{C}$. (b) Depth 19 mm. $T_{\max} = 31.1^{\circ}\text{C}$. (c) Depth 33 mm. $T_{\max} = 32.3^{\circ}\text{C}$. (d) Depth 38 mm. $T_{\max} = 26.1^{\circ}\text{C}$.

6. CONCLUSION

Two variants of a small sized ($45 \times 90 \text{ mm}^2$ chassis dimensions) radiometer frontend were investigated for medical applications. Both designs were shown to be stable as the stability factor $\mu > 1$ for all frequencies. The design with an LNA before the switch showed 36% higher sensitivity than the design with the Dicke switch in front. The design with an LNA before the switch can not be used during heating because of saturation problems during operation. The possibility to read temperature non-invasively at depth during interspersed heating and radiometric monitoring were also demonstrated in a phantom experiment.

ACKNOWLEDGMENT

Øystein Klemetsen is grateful to have had the opportunity to spend the academic year 2009-2010 at Duke University Medical Center in Durham, NC, USA. He also acknowledges the opportunity to enter

into an ongoing project between Duke University Medical Center and ThermImage in Salt Lake City.

REFERENCES

1. Mizushina, S., H. Ohba, K. Abe, S. Mizoshira, and T. Sugiura, "Recent trends in medical microwave radiometry," *IEICE Trans. Commun.*, Vol. E78-B, No. 6, 789–798, 1995.
2. Bardati, F. and S. Iudicello, "Modeling the visibility of breast malignancy by a microwave radiometer," *IEEE Transactions on Biomedical Engineering*, Vol. 55, No. 1, 214–221, Jan. 2008.
3. Arunachalam, K., P. R. Stauffer, P. F. Maccarini, S. Jacobsen, and F. Sterzer, "Characterization of a digital microwave radiometry system for noninvasive thermometry using a temperature-controlled homogeneous test load," *Physics in Medicine and Biology*, Vol. 53, No. 14, 2008.
4. Arunachalam, K., P. F. Maccarini, V. D. Luca, F. Bardati, B. W. Snow, and P. R. Stauffer, "Modeling the detectability of vesicoureteral reflux using microwave radiometry," *Physics in Medicine and Biology*, Vol. 55, No. 18, 5417, 2010.
5. Aitken, G. J. M., "A new correlation radiometer," *IEEE Transactions on Antennas and Propagation*, Vol. 16, No. 2, Mar. 1968.
6. Ulaby, F., R. Moore, and A. Fung, *Microwave Remote Sensing Fundamentals and Radiometry*, 1st Edition, Vol. 1, Artech House, 685 Canton Street, Norwood, MA 02062, USA, 1981.
7. Jacobsen, S. and O. Klemetsen, "Improved detectability in medical microwave radio-thermometers as obtained by active antennas," *IEEE Transactions on Biomedical Engineering*, Vol. 55, No. 12, 2778–2785, Dec. 2008.
8. Edwards, M. and J. Sinsky, "A new criterion for linear 2-port stability using a single geometrically derived parameter," *IEEE Trans. Microw. Theory Tech.*, Vol. 40, No. 12, 2303–2311, Dec. 1992.
9. Allan, D. W., "Should classical variance be used as a basic measure in standards metrology?" *IEEE Trans. Instrum. Measurements*, Vol. 36, No. 2, 646–654, 1987.
10. Land, D. V., A. P. Levick, and J. W. Hand, "The use of the allan deviation for the measurement of the noise and drift performance of microwave radioemeters," *Measurement Science Technology*, Vol. 18, No. 7, 1917–1928, 2007.

11. Barnes, J. A., A. R. Chi, L. S. Cutler, D. J. Healey, D. B. Leeson, T. E. McGunical, J. A. Mullen, W. L. Smith, R. L. Sydnor, R. F. C. Vessot, and G. M. R. Winkler, "Characterization of frequency stability," *IEEE Trans. Instrum. Measurements*, Vol. 20, No. 2, 105–120, 1971.
12. Bocquet, B., J. C. van de Velde, A. Mamouni, Y. Leroy, G. Giaux, J. Delannoy, and D. Delvaley, "Microwave radiometric imaging at 3 GHz for the exploration of breast tumors," *IEEE Trans. Microw. Theory Tech.*, Vol. 38, No. 6, 791–793, Jun. 1990.
13. Stauffer, P., F. Rossetto, M. Leencini, and G. Gentilli, "Radiation patterns of dual concentric conductor microstrip antennas for superficial hyperthermia," *IEEE Transactions on Biomedical Engineering*, Vol. 45, No. 5, 605–613, May 1998.
14. Maccarini, P., K. Arunachalam, T. Juang, V. De Luca, S. Rangarao, D. Neumann, C. Martins, O. Craciunescu, and P. Stauffer, "Shaping and resizing of multifed slot radiators used in conformal microwave antenna arrays for hyperthermia treatment of large superficial diseases," 746–749, Sep. 2009.
15. Brelum, S. H., "A numerical study of planar elliptical antennas applied to ultrawideband (UWB) imaging of breast tissue," LAP LAMBERT Academic Publishing, 2010.
16. Jacobsen, S. and P. Stauffer, "Nonparametric 1-D temperature restoration in lossy media using tikonov regularization in sparse radiometry data," *IEEE Transactions on Biomedical Engineering*, Vol. 50, No. 2, 178–188, Feb. 2003.